Journal of Applied Polymer Science

Crystallization and Thermal Properties of Biodegradable Polyurethanes Based on Poly[(R)-3-hydroxybutyrate] and Their Composites with Chitin Whiskers

Gamal R. Saad, Hend E. Salama, Nadia A. Mohamed, Magdy W. Sabaa
Chemistry Department, Faculty of Science, Cairo University, Giza, Egypt
Correspondence to: G. R. Saad (E-mail: grsaad@yahoo.com)

ABSTRACT: A series of biodegradable polyurethanes (PUs) were synthesized from hydroxylated bacterial poly[(R)-3-hydroxybutyrate], P[(R)-HB]-diol, as crystallizable hard segment and hydroxyl-terminated synthetic poly[(R,S)-3-hydroxybutyrate), P[(R,S)-HB]-diol, as an amorphous soft segment, using 1,6-hexamethylene diisocyanate, as non-toxic connecting agent. The P[(R)-HB] content was varied from 30 to 70 wt %. The resulting copolymers were characterized by FT-IR, ^{1}H-NMR, DSC, and TGA. The DSC data revealed that the melting of P[(R)-HB] segment increases with increasing its own content in the PUs. The cold and melt crystallization are enhanced with increasing P[(R)-HB] content. The TGA data revealed that the thermal decomposition mainly occurred via a single degradation step and the thermal stability slightly increased with increasing P[(R)-HB] content. The non-isothermal crystallization behavior of PU sample containing 40 wt % PHB with and without α-Chitin whiskers was studied using DSC, and their kinetics data were investigated via the Avrami, Ozawa, and Z.S. Mo methods, respectively. Crystallization activation energy was estimated using Kissinger's method. © 2014 Wiley Periodicals, Inc. J. Appl. Polym. Sci. **2014**, *131*, 40784.

KEYWORDS: biodegradable; crystallization; degradation; differential scanning calorimetry (DSC); polyurethanes

Received 17 January 2014; accepted 28 March 2014
DOI: 10.1002/app.40784

INTRODUCTION

In recent years, biodegradable plastics have attracted attention due to their environmental compatibility. Poly[(R)-3-hydroxybutyrate], P[(R-HB], appears to nearly ideally to meet such criteria.[1–3] It is produced biologically from renewable resources.[4] It is stable under normal usage conditions, but degrades rapidly on composting conditions. Additionally, PHB is the basis for biocompatible materials, and its degradation yields valuable stereoregular building blocks for organic synthesis. However, the shortcoming of brittleness and narrow processability window has limited the wide applications of PHB. These are mainly related to its relatively high melting temperature and high crystallinity.[5–7] Many approaches have been reported to improve the brittleness of PHB, for example, incorporation of other 3-hydroxyalkanoate units such as 3-hydroxyvalerate in the backbone of P[(R)-HB],[8–10] addition of plasticizers and nucleating agents,[11–13] blending with flexible polymers,[14] and copolymerization with flexible synthetic biodegradable components such as poly(ε-caprolactone) (PCL), poly(butylene adipate) (PBA), poly(diethylene glycol adipate) (PDEGA), or poly(ethylene glycol).[15–24] The advantage of the obtained copolymers over the other kinds of PHB material is that their segmented and domain structure can be easily controlled by a selection of the monomer units for building the segments, their relative proportions and the length of segments. Furthermore, many investigations have been conducted on compounding of P[(R)-HB] with nano-particles to improve the mechanical and thermal properties of neat P[(R)-HB].[25–29]

It is well known that the physical properties and biodegradability of biodegradable polymers are influenced strongly by the crystallinity. Meanwhile, the crystalline structure and morphology are also greatly influenced by the thermal history.[25–32] Therefore, the crystallization kinetics study should be paid enough attention, since it is not only affects the crystalline structure and morphology of semi-crystalline polymers, but also affects the final mechanical and physical properties and biodegradability. Crystallization during polymer processing occurs non-isothermally, except for some special cases. In order to reach optimizing condition in an industrial process and to obtain a product with desired properties, it is necessary to have some quantitative evaluations of the non-isothermal process.

From the above considerations, we present, herein, at first the synthesis and characterization of a series of segmented poly(ester-urethane)s (PUs) based on a crystallizable blocks of bacterial poly(R-3-hydroxybutyrate) P[(R)-HB] and amorphous

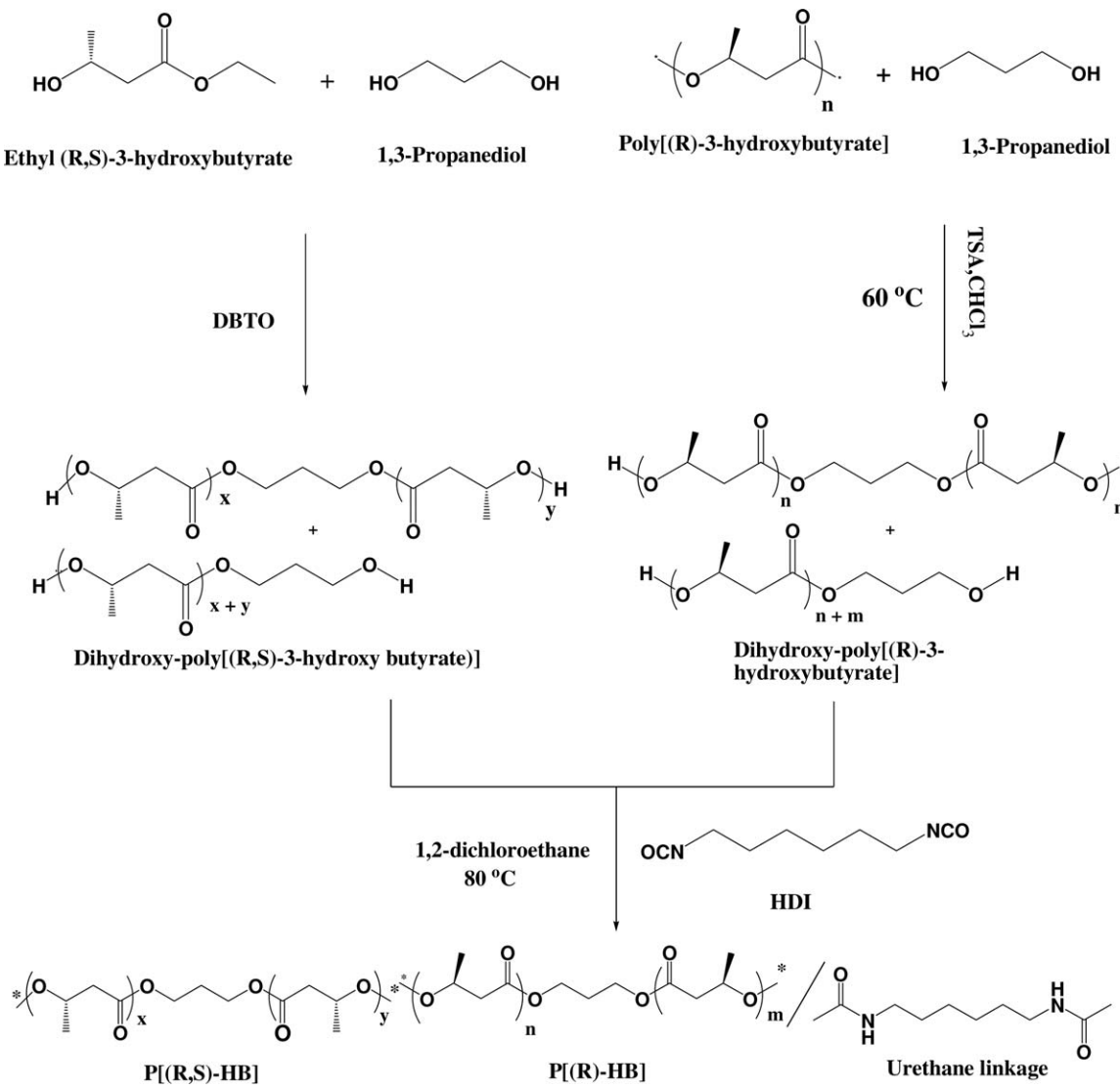

Scheme 1. Synthetic route of P[(R)-HB]-diol, P[(R,S)-HB]-diol and polyurethanes.

chemo-synthetic poly[(R,S)−3-hydroxybutyrate] P[(R,S)-HB] using 1,6-hexamethylene diisocyanate (HDI) as non-toxic connecting units. As the α-chitin whisker is a natural product and it is safe and environment-friendly,[33,34] the α-chitin whiskers is expected to be ideal candidate as a reinforcing and nucleating agent of the prepared neat PUs. Therefore, the non-isothermal crystallization and melting behavior of PHB segments in PUs with and without α-Chitin whisker (CW) was studied.

EXPERIMENTAL

Materials

Bacterial poly[(R)-3-hydroxybutyrate], PHB, was obtained from Coper sucar, Piracicaba, Brazil. 1,3-Propanediol, ethyl (R,S)-3-

Table I. Chemical Compositions and Molecular Weights of the Prepared Poly(ester-urethane)s

	Composition				
Sample code	P[(R)-HB] (wt %)	P[(R,S)-HB] (wt %)	Urethane linkage (wt %)	$\bar{M}_w$ (g/mol)	$\bar{M}_w/\bar{M}_n$
U[P(R)-HB]-30	30.0	59.2	10.8	84,000	2.6
U[P(R)-HB]-40	40.0	49.9	10.1	87,500	2.3
U[P(R)-HB]-50	50.0	40.8	9.2	81,300	2.1
U[P(R)-HB]-60	60.0	31.6	8.4	80,500	2.3
U[P(R)-HB]-70	70.0	22.4	7.62	72,000	2.2

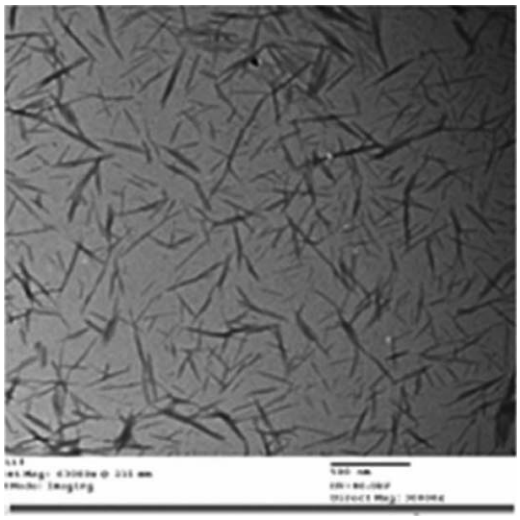

Figure 1. TEM images of a dilute suspension of chitin whiskers.

hydroxybutyrate, *p*-toluenesulphonic acid; 1-6-hexamethylene diisocyanate, all of synthetic grade were obtained from Fulka, Germany. The catalysts dibutyltin dilaurate and dibutyltin oxide were also obtained from Fluka. 1,2-Dichloroethane and dioxane were obtained from Aldrich. Ethyl (R,S)-3-hydroxybutyrate (Fluka) was distilled from molecular sieves 4 Å under vacuum prior to use. Chitin was obtained from Funakashi (Japan).

Pre-Polymers and Copolymer Synthesis

Hydroxy-terminated poly[(R)-3-hydroxybutyrate], P[(R)-HB]-diol, $\bar{M}_n = 2800$ g/mol and $\bar{M}_w/\bar{M}_n = 1.54$) was prepared by transesterification of high molecular weight poly[(R)-3-hydroxybutyrate] ($\bar{M}_n = 58{,}000$ g/mol and $\bar{M}_w/\bar{M}_n = 2.3$) with 1,3-propanediol in $CHCl_3$ at 60°C with *p*-toluenesulphonic acid as catalyst according to the method described previously.[18]

Hydroxy-terminated poly[(R,S)-3-hydroxybutyrate] P[(R,S)-HB]-diol, $\bar{M}_n = 1100$ g/mol and $\bar{M}_w/\bar{M}_n = 1.23$) was synthesized according to the method described previously.[35] In a two-necked round-bottom flask equipped with a distillation device 66.0 g (0.05 mol) fresh distilled ethyl (R,S)-3-hydroxybutyrate, 4.5 g (0.05 mol) 1,3-propanediol, and 0.62 g (2.5 mmol) *n*-dibutyltin oxide (DBTO), as the catalyst, were introduced. The reaction mixture was initially heated under a gentle stream of argon at 100°C for 3 h and ethanol was recovered by distillation. Then, the reaction mixture was heated for further 5 h, at 110°C while gradually reduced the pressure to 0.5 mmHg. After the reaction was completed, the product was dissolved in a minimum amount of methylene chloride followed by precipitation into excess amount of n-hexane.

Poly(ester-urethane)s, PUs, were synthesized by one step polymerization reaction in solution from P[(R)-HB]-diol, as hard segments, and P[(R,S)-HB]-diol, as soft segments using stoichiometric amounts of 1,6-hexamethylene diisocyanate (HDI) as a coupling agent. Solution polymerization was performed by the method described previously[18] using 1,2-dichloroethane as the solvent and dibutyltin dilaurate as the catalyst, as represented in Scheme 1. The relative amounts of the reaction mixture were adjusted, so that the resulting polymer would contain from ~30 to ~70 wt % P[(R)-HB]. The copolymers were separated in high yields (>95%) by precipitation in excess amount of low boiling petroleum ether. The isolated polymers were purified by the dissolution in dioxane and re-precipitation in distilled water and dried under vacuum at room temperature for at least 48 h.

The chemical compositions and molecular weights of the synthesized poly(ester-urethane)s are given in Table I. In this study, each copolymer is designated by a code, related to the structure of the hard segment, followed by a number indicating the content of P[(R)-HB] hard segment in wt %.

Preparation of Chitin Whiskers (CW)

Chitin whiskers were produced using the procedure described previously.[36] The purified chitin sample was hydrolyzed using 3 *N* HCl at the boil for 1.5 h under stirring. The ratio of 3 *N* HCl to chitin was 30 mL/g. After acid hydrolysis, the suspension was diluted with distilled water followed by centrifugation (10,000 rpm for 5 min). This process was repeated three times. Next, the suspensions were transferred to a dialysis tube and dialyzed for 24 h against distilled water until a pH = 6 was reached, then was freeze-dried.

TEM micrograph of chitin whiskers (CW) represented in Figure 1 shows the homogeneity and nanometric dimensions of chitin whiskers. The mean diameter (d) of prepared chitin whiskers is about 18 nm and the mean length (L) is 216 nm. Therefore, the aspect ratio $(L/d)$of CW estimated from TEM is about 12.

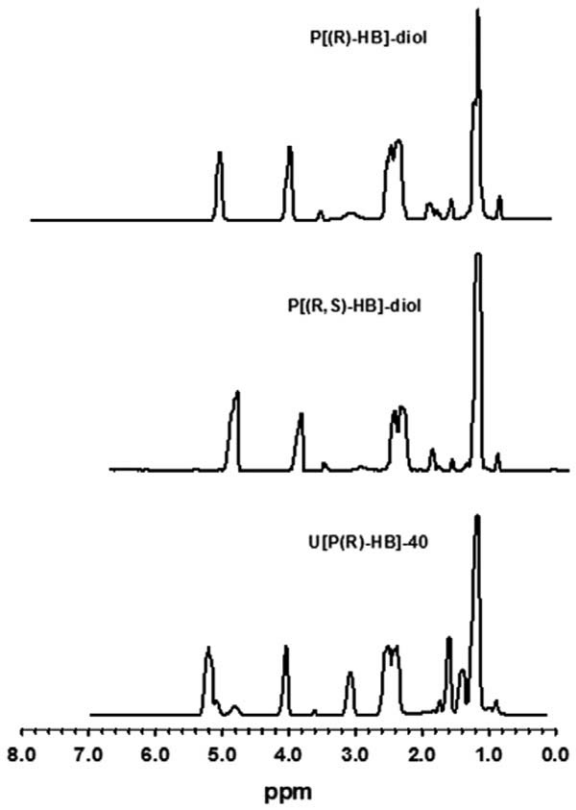

Figure 2. ^{1}H-NMR spectra of P[(R)-HB]-diol, P[(R,S)-HB]-diol, and U[P(R)-HB]-40.

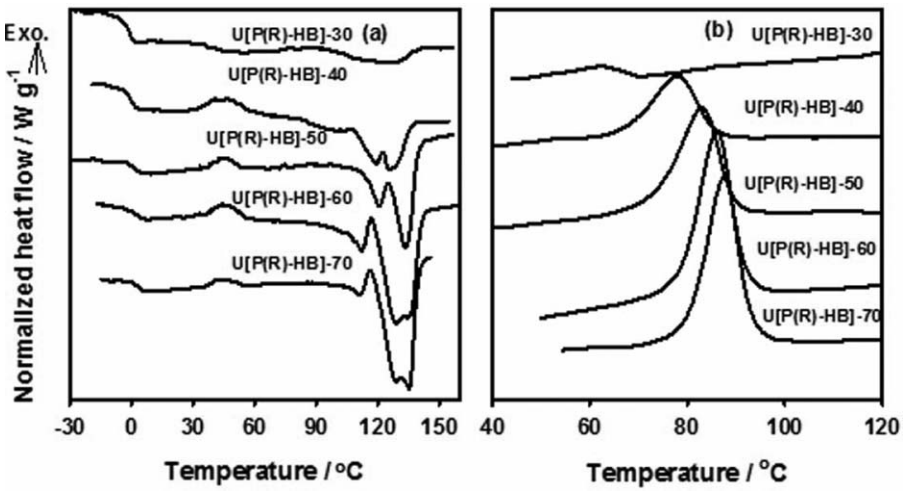

Figure 3. DSC scans of PUs (a) reheated after rapid cooling, (b) cooling from melt.

Preparation of PUs/Chitin Whiskers Composites

The neat PUs was dissolved in dioxane, and then an appropriate weight of chitin whiskers suspensions in dioxane was added with stirring. The suspensions were sonicated for 2 min before being cast in Teflon molds, where the films were obtained by solvent evaporation in a vacuum oven at 80°C for 48 h. The content of the chitin whiskers of the produced films was 1, 3, and 5 wt %.

Characterization

FTIR Infrared analysis was carried out between 400 and 4000 cm^{-1} using a Perkin-Elmer B25 spectrophotometer. All measurements were carried out with 64 scans at resolution of 2 cm^{-1} at room temperature.

^{1}H-NMR spectra were recorded on a Bruker AC-400 in $CDCl_3$. Non-deuterated $CHCl_3$ was used as the internal reference.

The molecular weight data were obtained by Gel-Permeation Chromatography (GPC) at 30°C, using a Waters model 510 and a model 410 refractive index detector with 10^3-10^5 ultrastyragel column connected in series. Chloroform was used as eluent with a flow rate of 1.5 cm^3/min, and sample concentrations of 20 mg/cm^3. Polystyrene standards with low dispersity (Polystandard series, Mainz, Germany) were used to construct a molecular weight calibration curve.

SEM images were obtained using JEOL (JSM-5200) scanning electron microscope. Samples were prepared by placing small part of film on a carbon tape on a stub, which was coated with a thin layer of gold.

TEM image of chitin whiskers was obtained with Transmission Electron Microscope JEOL (JEM-1400 TEM) using an acceleration voltage of 100 kV. A drop of diluted suspension of chitin whiskers was deposited and dried on a carbon-coated grid and then measured.

Thermal degradation studies were conducted under nitrogen with dynamic heating rate of 10°C/min using Shimadzu TGA-50 H Thermal Analyzer. All experiments were conducted from room temperature to 600°C and the reference material was α–alumina. The sample weights in all experiments were taken in the range 2–4 mg.

Wide-angle X-ray diffraction (WAXD) measurements were performed at room temperature using a Philips Xpert MPD Pro diffractometer, equipped with Ni-filtered Cu-Kα radiation ($\lambda = 0.154$ nm) at an accelerating voltage/current of 50 kV/40 mA. The 2θ scan range was used from 3° to 70° at a scan speed of 1 step s^{-1}.

PL-DSC (Polymer-Laboratories, England, UK) Differential Scanning Calorimeter was employed to study the glass transition

Table II. Thermal Characteristic Parameters of Pus

Sample code	T_g[a] (°C)	T_{cc}[a] (°C)	T_{mc}[b] (°C)	T_m[a] (°C)	ΔH_m[a] (J/g)	X_c[c] (%)	$T_{5\%}$ (°C)	$T_{max.}$ (°C)
U[P(R)-HB]-30	−2	84	63	120, 127	16.7	38.0	225	261
U[P(R)-HB]-40	−1	48	78	119, 128	28.1	48.1	225	261
U[P(R)-HB]-50	2	45	83	121, 132	36.0	49.4	236	263
U[P(R)-HB]-60	2	44	86	113, 133	46.0	52.5	237	266
U[P(R)-HB]-70	4	45	88	112, 134	55.6	54.4	241	269

[a] Determined from reheating scan after rapid cooling (Run II).
[b] Determined from cooling scan of melt samples (Run III).
[c] Crystallinity percentage according to the following equation: $X_c = 100 \times \Delta H_m / w_i \times \Delta H_m$, where ΔH_m is the melting enthalpy of P[(R)-HB] and ΔH_m is the melting point enthalpy of completely crystallized PHB with reference values of 146 J/g, w_i is the weight fraction of P[(R)-HB] in the copolymers.

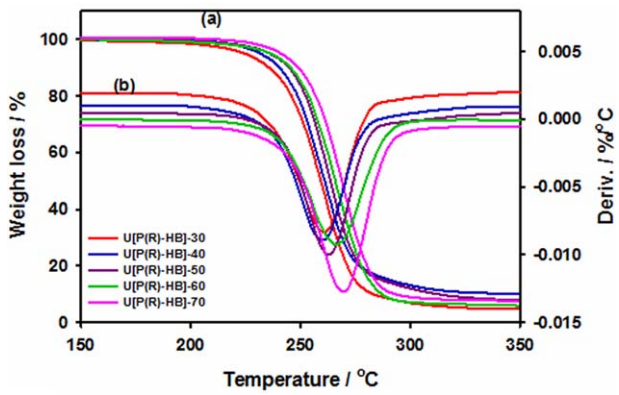

Figure 4. TG and DTG thermograms obtained from investigated PUs. [Color figure can be viewed in the online issue, which is available at wileyonlinelibrary.com.]

temperature (T_g), melting (T_m), and crystallization behavior of polymers. The calorimeter was calibrated with ultra-pure indium. Samples (10–12 mg) were first heated from −40 to 170°C with a heating rate of 10°C/min (Run I). After keeping them at 170°C for 2 min, samples were rapidly cooled to −60°C at a rate of 60°C/min to obtain specimen with low crystallinity, and then heated again with a heating rate of 10°C/min to 170°C (Run II). The melting temperature (T_m) and the cold crystallization temperature (T_{cc}) were taken as the peak values of the respective endotherm and exotherm processes in DSC thermograms. The apparent melting enthalpy (ΔH_m) was determined from the area of the endothermic peaks. The glass transition temperature (T_g) was taken as the midpoint of the specific heat capacity. The cooling curve run (III) was scanned over the temperature range from 170°C to −60°C at a constant rate of 10°C/min. The melt crystallization temperature (T_{mc}) was determined from the exotherm peaks in this run.

For observing the effects of the cooling rates on the non-isothermal melt-crystallization behavior of the polymer, the samples were melted at 170°C for 2 min then cooled at a given rate. The cooling rate used in this study ranged from 5, 10, 15, and 20°C/min. The exothermic crystallization peak was recorded as a function of temperature. The relative degree of crystallinity, $X(T)$, as a function of crystallization temperature T are defined as

$$X(T)=\int_{T_0}^{T}(\partial H/\partial T)dT/\int_{T_0}^{T_\infty}(\partial H/\partial T)dT$$

where δH is the enthalpy of crystallization released in infinitesimal temperature range δT, and T_0 and T_∞ are the temperatures at which crystallization starts and ends, respectively.

RESULTS AND DISCUSSION

Synthesis and Characterization

PUs were synthesized from bacterial P[(R)-HB]-diol, as hard segments, and chemo-synthetic P[(R,S)-HB]-diol, as soft segments, using 1,6-hexamethylene diisocyanate, as a non toxic connecting agent, in one step polymerization following the synthetic route as outlined in Scheme 1. The content of P[(R)-HB] systematically varied from ~30 to ~70 wt %. As shown in Table I, the molecular weight of the resulting PUs decreases with increasing the P[(R)-HB] content, except polyurethane sample containing ~40 wt % P[(R)-HB]. This might result from the formation of a small fraction of PHB macrodiols with non-reactive end groups, as a result of crotonization.[16,18] The chemical structure of the synthesized P[(R)-HB]/P[(R,S)-HB] PUs was analyzed by FT-IR and ^{1}H-NMR. All the characteristic absorptions of P[(R)-HB] and P[(R,S)-HB] segments can be clearly discerned in the FT-IR spectra of the synthesized PUs. The most significant peak appearing at 1725 cm^{-1} is assigned to C═O stretching of the ester groups of P[(R)-HB] repeating units of the crystalline fraction, while the stretching of C═O of amorphous fraction of P[(R)-HB] and amorphous P[(R,S)-HB] appears at 1730 cm^{-1}.[37] The two absorption bands appear at 1528 and 3400 cm^{-1} are assigned to NH deformation and stretching modes of the urethane linkage,[38] respectively. The methylene –CH stretching of P[(R)-HB] repeating units and urethane linkages appear at 2980 cm^{-1}. ^{1}H-NMR spectra of PUs U[(R)-HB]-40, as a representative example, shows the corresponding resonance of hydrogen protons resulting from PUs

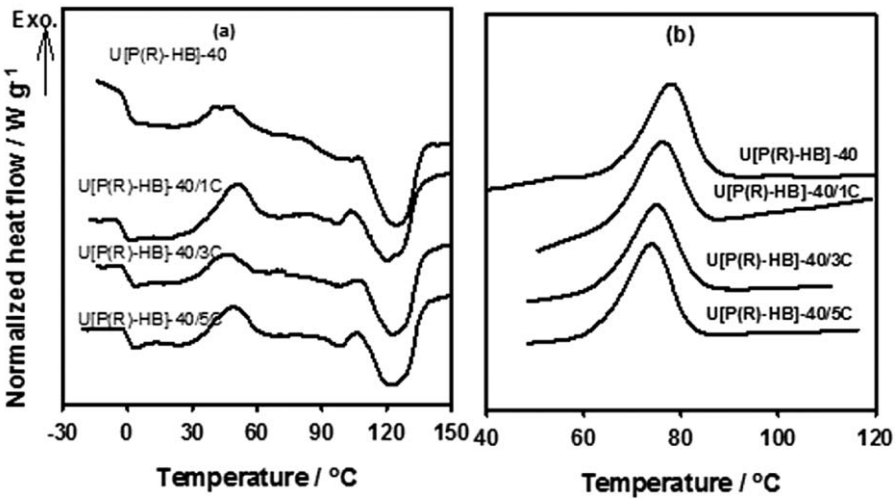

Figure 5. DSC scans of U[P(R)-HB]-40 and its U[P(R)-HB]-40/CW composites (a) reheated after rapid cooling, (b) cooling from melt.

Table III. Thermal Characteristic Parameters of U[P(R)-HB]-40 and U[P(R)-HB]-40/Chitin Whiskers Nanocomposites

Sample code	T_g[a] (°C)	T_{cc}[a] (°C)	T_{mc}[b] (°C)	T_m[a] (°C)	ΔH_m[a] (J/g)	X_c[c] (%)	T5% (°C)	$T_{max.}$ (°C)
U[P(R)-HB]-40/1C	−2	51	76	99,122	26.5	45.4	236	263
U[P(R)-HB]-40/3C	0	46	75	98,123	25.3	43.3	242	268
U[P(R)-HB]-40/5C	1	49	74	99,122	24.7	42.3	247	271

[a] Determined from reheating scan (Run II) after rapid cooling.
[b] Determined from cooling scans of melt samples (Run III)
[c] Crystallinity percentage according to the following equation: $X_c = 100 \times \Delta H_m/w_i \times \Delta H_m$, where ΔH_m is the melting enthalpy of PHB and ΔH_m is the melting point enthalpy of completely crystallized P[(R)-HB] with reference values of 146 J/g, w_i is the weight fraction of PHB in the copolymer composites.

structure (Figure 2). The proton signals at 5.25 ppm were assigned to the methine –OCH– of both P[(R)-HB] and P[(R,S)-HB] repeating units, while the proton resonance of corresponding to methylene groups –OCH_2– is observed at 2.40–2.68 ppm. The appearance of –NH– resonance at 4.80 ppm and disappearance of P[(R,S)-HB] and P[(R)-HB] terminated hydroxy groups at 3.20 ppm confirms the formation of PUs. The resonance appearing at 3.10 ppm ascribed to the methylene groups adjacent to the urethane –NH–, and the protons resonance at 1.45 ppm, originating from the middle methylene of the urethane linkage units, could all be clearly distinguished.

Thermal Properties of PUs

The thermal transition, crystallization, and melting behaviors of the PUs with different compositions were initially studied by DSC. The DSC scans are represented in Figure 3. The values of glass transition temperature (T_g), melting point (T_m), fusion enthalpy (ΔH_m), and cold crystallization temperature (T_{cc}) were obtained from heating scans after rapid cooling (Run II), and melt crystallization temperature (T_{mc}) was obtained from cooling scans (Run III). The results are summarized in Table II. It is obvious from Figure 3(a) that the PUs exhibit a single glass transition temperature, being similar to that of T_g of high molecular weight bacterial P[(R)-HB] and P[(R,S)-HB] homopolymers.[39,40] The T_g slightly shifts to higher temperatures with increasing weight fraction of the PHB. Above the T_g, a small exotherm crystallization is obseved, followed by a more intense endotherm double melting peaks corresponding to crystallization and melting of PHB segments, respectively. Such an increase in areas under the melting peak indicates that a considerable crystallization has occurred during the rapid cooling process from the melts. For U[P(R)-HB]-30 sample, the cold crystallization peak is difficult to detect. The crystallization peak shifts to higher temperature as the P[(R,S)-HB] content increase. This suggests that the P[(R,S)-HB] segments reduce the stereoregularity of bacterial PHB segments and the crystallization is restricted to certain degree. The endotherm shown at lower temperature can be attributed to the incomplete crystals of PHB component in the copolymer that can recrystallize on melting. The higher melting endotherm is corresponding to the perfect PHB crystalline phase.[41] Also the results reveal that T_m increases with increasing PHB content. The crystallinity of the samples was determined from the melting enthalpy ratios (ΔH_m^o), assuming that the enthalpy of 100% crystalline PHB is 146 J g^{-1}.[42] The results of DSC (Table II) show that the degree of crystallinity decreases with the increasing of P[(R)-HB] content. Figure 3(b) shows the non isothermal crystallization of PUs at a cooling rate 10°C/min. From this figure and Table II, it can be seen that the melt crystallization peak (T_{mc}) shifts to higher temperature with increasing weight fraction of P[(R)-HB], indicating that the crystallization rate of PHB enhances with increasing its content in the copolymers.

Figure 4 illustrates the TG and DTG curves of PUs. From these curves, the thermal stability parameters including, the onset decomposition temperature, which is defined as the temperature

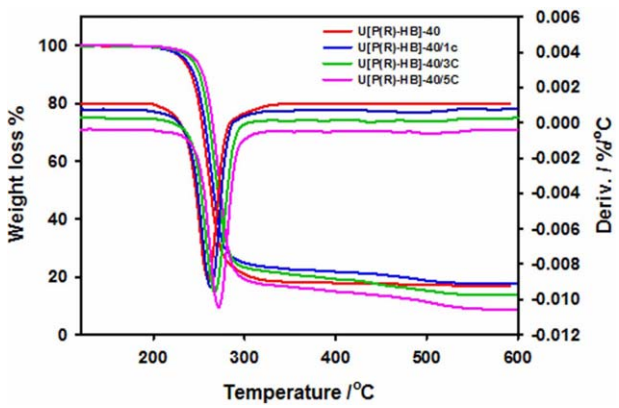

Figure 6. TG and DTG thermograms obtained from U[P(R)-HB]-40 and its UPHB/CW composites. [Color figure can be viewed in the online issue, which is available at wileyonlinelibrary.com.]

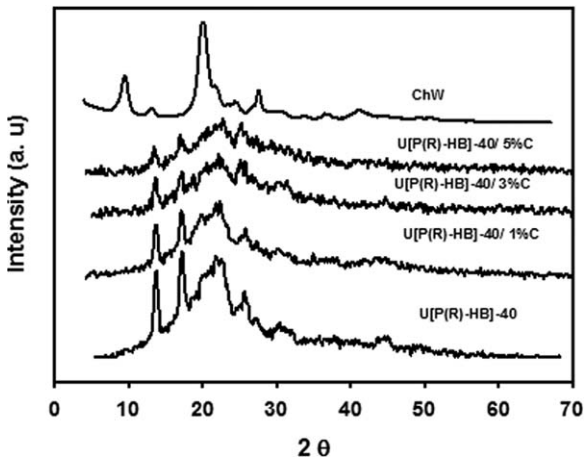

Figure 7. X-ray diffraction curves of pure U[P(R)-HB]-40/CW and U[P(R)-HB]40/CW nanocomposites.

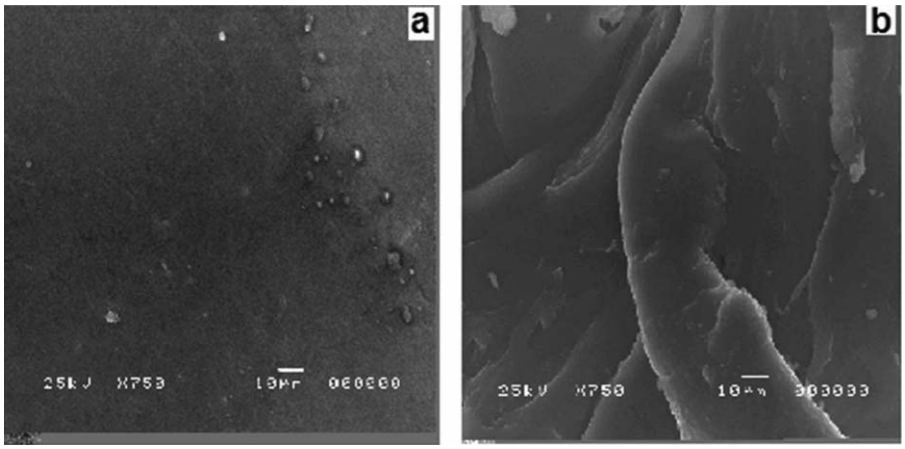

Figure 8. SEM images of fractured surfaces of (a) U[P(R)-HB]-40 and (b) U[P(R)-HB]-40/3 wt % CW.

at 5% weight loss ($T_{5\%}$) and the temperature of maximum weight loss (T_{max}) are included in Table II. All investigated samples exhibit a single-step decomposition between 220 and 300°C, as clearly indicated by their single DTG peak. This degradation step is assigned to the degradation of P[(R)-HB] and P[(R,S)-HB] segments.[43] As seen in Table II, the $T_{5\%}$ and T_{max} increase with increasing P[(R)-HB] weight fraction. This indicates that the thermal stability of the investigated PUs is improved as the P[(R)-HB] hard segments content increase, and consequently widening the processing window.

Influence of Chitin Whiskers on the Thermal Properties of PUs

The DSC scans of the U[P(R)-HB]-40 and its composites containing 1, 3, and 5 wt % chitin whiskers (CW) are displayed in Figure 5 and the derived thermal parameters are summarized in Table III. Compared with neat UP[(R)-HB]-40, it is obvious that the T_{cc} of nanocomposite loaded with 1% CW shifts to a higher temperature by 3°C, while it decreases about 2°C with the incorporation of 3% CW. On the other hand, increasing CW up to 5% shows insignificant effect on T_{cc}. Actually, the crystallization behavior of the polymer nanocomposites is complex since several superimposed phenomena may occur. In fact, there are mainly two factors controlling the crystallization rate of polymeric composite system. One is that the filler acts as nucleating agent, which enhances crystallization, and the other is that it hinders the migration and diffusion of polymer molecular chains to the surface of the nucleus, thus constrain the spherulitic growth by an impingement mechanism in the composites; this results in a negative effect on crystallization. From the aforementioned data, no conclusive result could be obtained regarding the influence of the CW amount on the cold crystalization behavior since T_{cc} insignificantly and irregularly changed with CW whiskers. One possible reason for such variation in the cold crystallization behavior may be ascribed to a variation in the dispersion in addition to the formation of CW aggregates within the polymer matrix in the frozen glassy state. It can also be observed from Table III that the T_g values of the nanocomposite are insignificantly affected with loading by various amounts of CW. Moreover, it is found that T_m values of all samples are unchanged, although the crystallinity decreases from 48.1 to 42.3% with the increase of CW from 0 to 5%, suggesting that the CW hinders chain mobility, and thus the

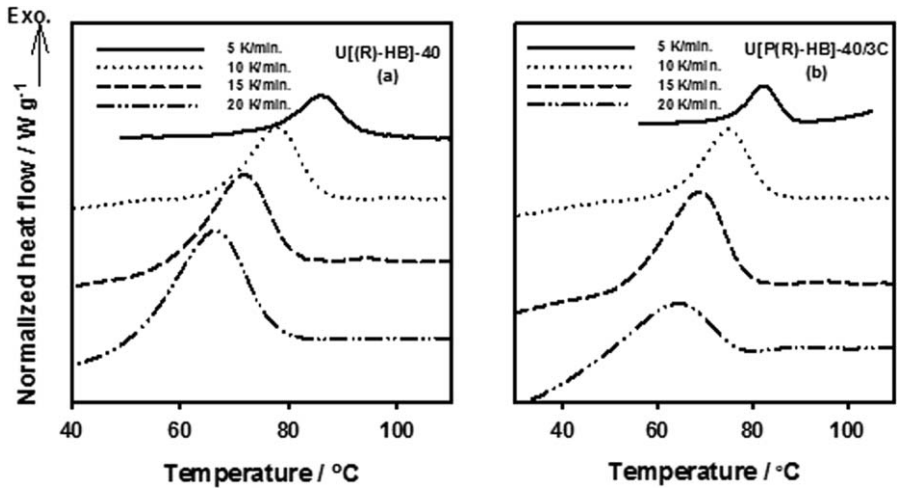

Figure 9. Non-isothermal melt-crystallization exotherm of (a) U[P(R)-HB]-40 and (b) U[P(R)-HB]-40/3 CW nanocomposite at different cooling rates.

Table IV. Kinetic Parameters of Non-Isothermal Crystallization of U[P(R)-HB]-40 and U[P(R)-HB]-40/3 C Composite

Sample code	ϕ (°C min^{-1})	T_p (°C)	ΔH_{mc} (J/g)	n	Z_t (min^{-n})	Z_c (min^{1-n} °C^{-1})	$t_{1/2}$ (min)
U[P(R)-HB]-40	5	86	−29.3	2.58	0.072	0.590	2.412 [2.410]
	10	78	−27.1	2.40	0.484	0.930	1.180 [1.162]
	15	72	−26.0	2.35	0.967	0.998	0.878 [0.868]
	20	67	−23.6	2.47	3.435	1.064	0.531 [0.523]
U[P(R)-HB]-40/3C	5	83	−26.3	2.15	0.125	0.673	2.242 [2.181]
	10	75	−25.1	2.75	0.308	0.890	1.349 [1.339]
	15	69	−21.1	2.45	0.759	0.982	0.978 [0.964]
	20	65	−19.2	2.36	2.710	0.994	0.786 [0.879]

crystallization of P[(R)-HB] segments in the copolymer is decreased. Analysis of the DSC cooling thermograms [Figure 5(b) and Table III] revealed that the nanocomposite exhibits a lower melt crystallization (T_{mc}) values compared with neat sample; this implies that the incorporation of CW within the polymer matrix retards the crystallization of the P[(R)-HB] segments from molten state.

The thermal stability of the polymer composites plays a crucial role in determining the limit of their working temperature and the environmental conditions for use. The representative TG and DTG curves obtained from U[P(R)-HB]-40 and its nanocomposites are shown in Figure 6 and the characteristics decomposition temperatures are appended in Table III. It can be seen that the thermal degradation profile of the composites is similar to that of neat sample and the characteristic decomposition temperatures, namely $T_{5\%}$ and the T_{max} of U[P(R)-HB]-40 increase with increasing the CW content. This implies that incorporation of CW into the polymer matrix improves the thermal stability of the matrix. Similar trend was observed by many researches in chitin whiskers reinforced polymers composites, especially when the content of CW was <10 wt %.[44–47]

Wide Angle X-ray Diffraction (WAXD) of U[P(R)-HB]-40 Nanocomposites

Figure 7 illustrates the WAXD patterns of pure U[P(R)-HB]-40, α-chitin whiskers (CW) and U[P(R)-HB]-40/CW composites containing different amounts of CW. Two strong diffraction peaks of the crystallite of the P[(R)-HB] segments are detected around 2 $\theta = 13.6°$ and 17.1° assigned to be (020) and (110) of the orthorhombic unit cell, respectively.[48,49] For CW, three main scattering intensity peaks can be identified at $2\theta = 9.4°$, 19.5°, and 27.3°, which are assigned to the (020), (100), and (130) reflexion planes of CW.[50,51] The characteristic peaks of both P[(R)-HB] and CW are observed in the X-ray diffraction patterns of the all U[P(R)-HB]-40 nanocomposites, which means that P[(R)-HB] and CW both can crystallize in the nanocomposite. As the amount of CW incorporated in U[P(R)-HB] matrix increased, the peaks of P[(R)-HB] become less sharper than those in the pure U[P(R)-HB]-40 and 2θ has some changes. The reason might be due to the impregnation of the CW into the copolymer matrix.

Morphology

Figure 8 shows the morphological features of fractured surfaces of the neat U[P(R)-HB]-40 and its nanocomposite loaded with

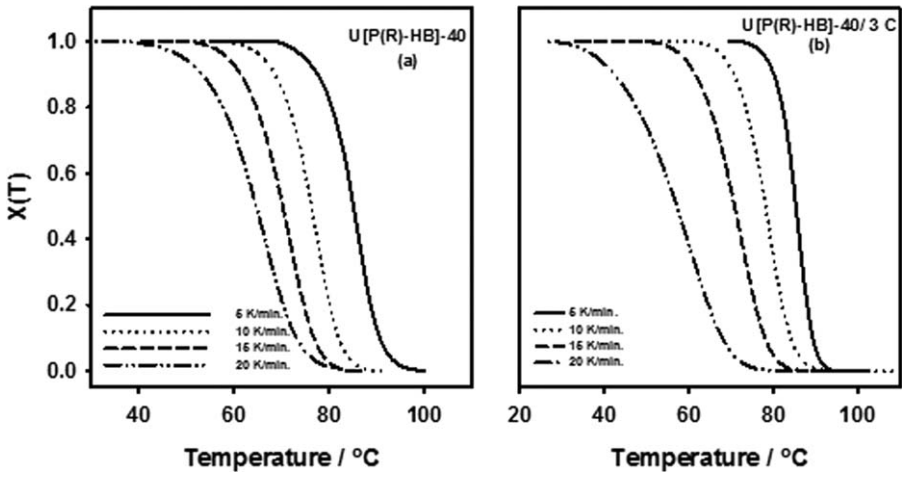

Figure 10. Relative crystallinity vs. temperature for non-isothermal crystallization of (a) U[P(R)-HB]-40 and (b) U[P(R)-HB]-40/3C composite at different cooling rates.

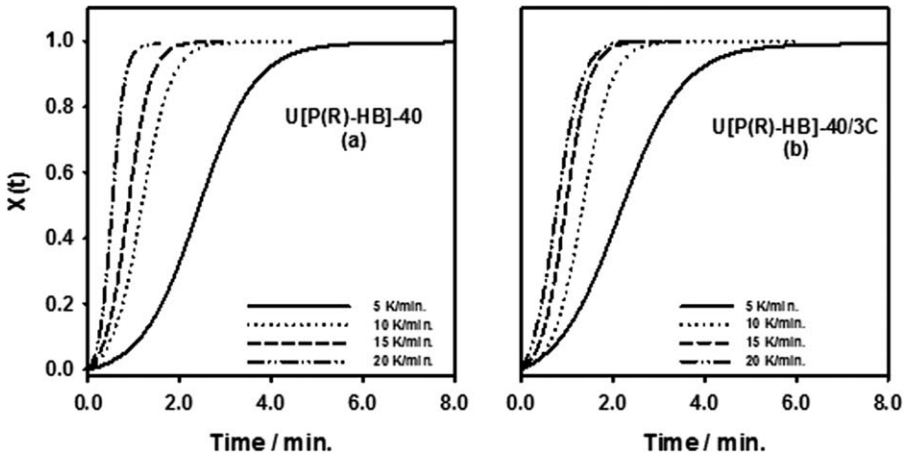

Figure 11. Relative crystallinity vs. time for non-isothermal crystallization of (a) U[P(R)-HB]-40 and (b) U[P(R)-HB]-40/3C composite at different cooling rates.

3.0 wt % CW. As seen from Figure 8(a), the surface morphology of neat U[P(R)-HB]-40 exhibited smooth surface, while UP[(R)-HB]-40/3 CW nanocomposite showed a fluctuant fractured surface [Figure 8(b)].

Non Isothermal Crystallization

In order to investigate the effect of chitin whiskers (3 wt %, was chosen as a representative example as it represents the moderate value between the investigated samples) on the kinetics of non-isothermal crystallization of the copolymer nanocomposite compared with pristine copolymer, we confind ourselves with copolymer sample possessing the highst molecular weight avaliable, namely U[P(R)-HB]-40 copolymer that contains 40 % of crystallizable P[(R)-HB] component. The non-isothermal crystallization exothermic peaks of U[P(R)-HB]-40 and U[P(R)-HB]-40/3 CW at various cooling rate are shown in Figure 9 and the kinetic parameters are summarized in Table IV. It is clearly seen that, as the cooling rate increases, the peak crystallization temperature T_p shifts to lower temperatures and the crystallization exotherm becomes wider for all the samples. This could be explained as follows: when the specimens are cooled with a lower rate during DSC scans, they have enough time to form necessary nuclei and to crystallize. So, the beginning of the crystallization exotherm appears at higher temperature. As the cooling rate increases, the motion of PHB segments in the copolymer chains cannot follow the cooling rate. Hence, the crystallization occurs at lower temperature. As seen in Table IV, the values of T_p of U[P(R)-HB]-40/ 3CW shifts to low temperature compared with neat U[P(R)-HB]-40 at a given cooling rate, which indicates that the CW can delay the melt-crystallization of PHB segments in the copolymer. The crystallization enthalpies (ΔH_{mc}) decrease gradually with increasing cooling rates for the samples investigated. Furthermore, the ΔH_{mc} of U[P(R)-HB]-40/3CW composite is lower than that of neat U[P(R)-HB]-40 at a given cooling rate, suggesting that the total crystallinity of the composite is declined by CW.

From DSC crystallization curves of U[P(R)-HB]-40 and U[P(R)-HB]-40/3 CW, the relative crystallinity as a function of temperature at different cooling rates is shown in Figure 10. The data can be further analyzed by converting the temperature scale of the *X(T)* function into the time scale to obtain the relative crystallinity function of time *X(t)*.

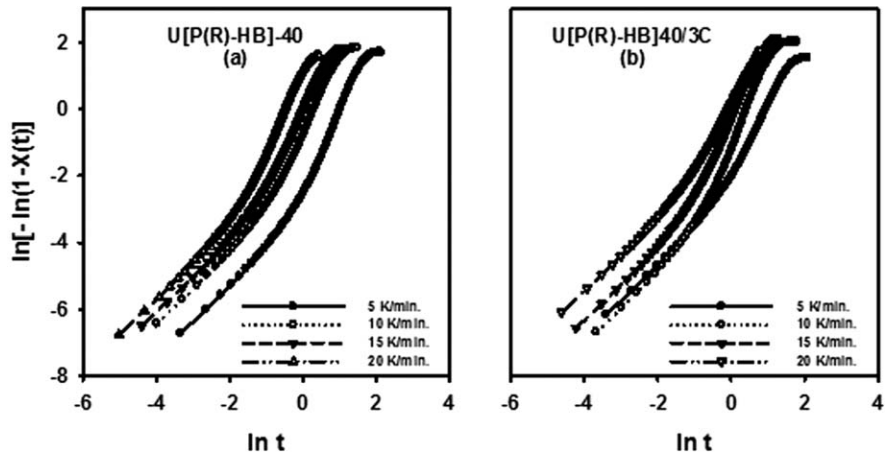

Figure 12. Plots of ln[−ln(1 − *X*(*t*)] versus ln *t* for (a) U[P(R)-HB]-40 and (b) U[P(R)-HB]-40/3C composite.

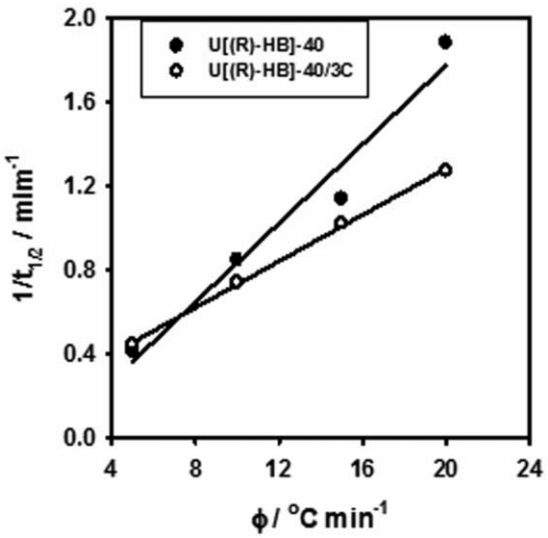

Figure 13. Plots of $1/t_{1/2}$ as a function of cooling rates.

The relation between crystallization time t and sample temperature T can be formulated as

$$t = \frac{(T_0 - T)}{\phi}$$

where T is the temperature at crystallization time t, T_0 is the temperature at which crystallization starts and ϕ is the cooling rate.

The converted curves are illustrated in Figure 11. All curves in Figures 10 and 11 have the similar sigmoidal or inverted sigmoidal shape.

The most common model to describe the overall nonisothermal crystallization kinetics is the modified Avrami equation, in which $X(t)$ can be expressed in the following form

$$\ln[-\ln(1-X(t)] = \ln Z_t + n \ln t \quad (1)$$

where Z_t and n are the Avrami crystallization rate constant and the Avrami exponent, respectively. Both Z_t and n are constants, specific to a given crystalline morphology and type of nucleation for a particular crystallization condition. Considering the temperature dependent character of the nonisothermal crystallization process investigated, Jeziorny pointed out that Z_t should be corrected as follows.[52]

$$\ln Z_c = \frac{\ln Z_t}{\phi} \quad (2)$$

By plotting $\ln[-\ln(1-X(t)]$ versus $\ln t$, as given in Figure 12, the kinetic parameters n and Z_t were obtained from the slope and intercept of the line, respectively, which are given in Table IV with the values of Z_c. In the fitting, the relative crystallinity data between 0.05 and 0.95 were used. As seen in Table IV, the n values were found to be in the range 2.15–2.58 and 2.15–2.75 for U[P(R)-HB]-40 and U[P(R)-HB]-40/3C, respectively, suggesting that the crystallization proceeds by three-dimension spherical growth. The overall rate parameter Z_c, determines both of the nucleating and growth processes, increase with increasing cooling rate, indicating a faster crystallization rate at a higher cooling rate. Z_t and Z_c, of the neat sample are slightly higher than that of composite at a given cooling rate, suggesting a slower crystallization rate of crystallizable of P[(R)-HB] segments in the presence of chitin whiskers.

Another important parameter is the half-time of crystallization ($t_{1/2}$), which is defined as the time at which the crystallinity is equal to 50%. In Avrami eq. (1), when $X(t) = 50\%$:

$$Z_t = \ln 2/(t_{1/2})^n \quad (3)$$

The dependence of $t_{1/2}$ on cooling rate (ϕ) for the investigated samples is listed in Table IV. With increasing ϕ, $t_{1/2}$ decreases accordingly both for neat U[P(R)-HB]-40 and its composite, indicating that the samples can crystallize more quickly at higher cooling rate. In addition, the half crystallization time $t_{1/2}$ calculated from eq. (3) (values between brackets) agrees with that obtained experimentally from Figure 11, suggesting that the Avrami equation analysis is adequate to describe the crystallization mechanism of PHB segments in U[P(R)-HB]-40 and its nanocomposite. By taking the inverse of $t_{1/2}$ a measurement of crystallization rate can be obtained and plotted versus the

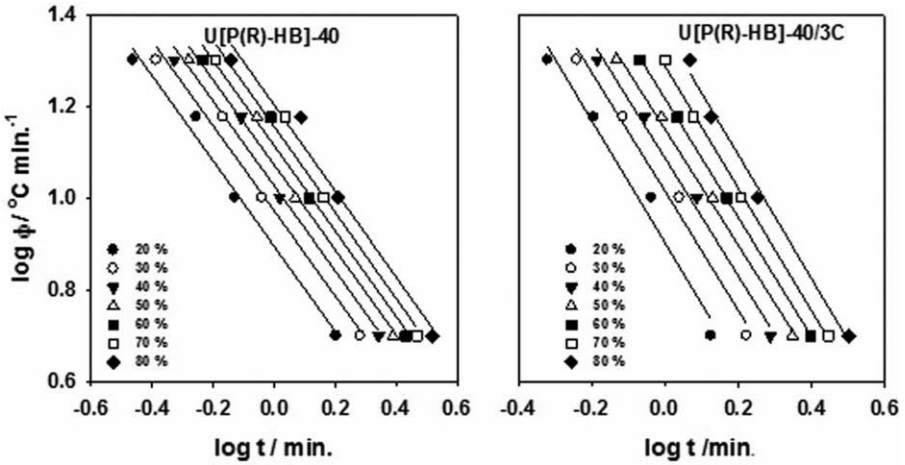

Figure 14. Plots of log ϕ versus log t for (a) U[P(R)-HB]-40 and (b) U[P(R)-HB]-40/3C at different crystallinity.

Table V. Nonisothermal Crystallization Kinetics Parameters of U[P(R)-HB]-40 and its U[P(R)-HB]-40/3C Composite at Different Degrees of Crystallinity by the Mo Method

	U[P(R)-HB]-40		U[P(R)-HB]-40/3C	
$X(T)$	log $F(T)$	a	log $F(T)$	a
20	0.895	0.931	0.903	1.333
30	0.972	0.927	1.015	1.295
40	1.027	0.926	1.087	1.282
50	1.072	0.926	1.151	1.265
60	1.115	0.933	1.217	1.297
70	1.156	0.938	1.288	1.334
80	1.203	0.940	1.365	1.350

heating rate in Figure 13. From this figure, it can be observed that the U[P(R)-HB]-40 composite exhibits the lower crystallization rate compared to the neat sample.

Ozawa took the effect of cooling rate on the non-isothermal crystallization into consideration and developed the Avrami equation to describe the nonisothermal crystallization as follows:

$$\ln[-\ln(1-X(T)] = \ln K(T) + m \ln \phi \quad (4)$$

$K(T)$ is called the heating function of the process, and m is the Ozawa component that depends on the crystal growth and nucleation mechanism.[53] We have tried to use this method to describe the crystallization kinetics of the investigated samples. yet no straight lines could be obtained when plotting ln $[-\ln(1 - X(T)]$ versus ln ϕ, suggesting that the Ozawa equation is unable to study the non-isothermal crystallization kinetics of the PUs. The Ozawa method sometimes is not usable in other polymers.[53–56]

The Mo method,[57] which is almost a universal method and is proved to be efficient to describe non-isothermal crystallization kinetics of many polymers,[58–61] is deduced from the Ozawa and Avrami equation. It was expressed as:

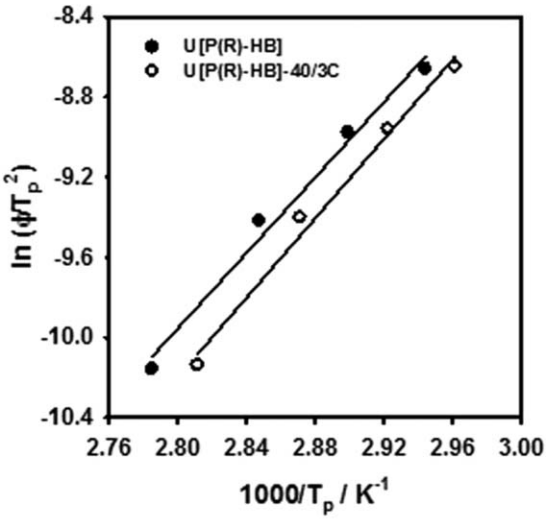

Figure 15. Plots of $\ln(\phi/T_p^2)$ versus $1/T_p$ for U[P(R)-HB]-40 and U[P(R)-HB]-40/3C composite.

$$\log \phi = \log F(T) + a \ln t \quad (5)$$

where $F(T) = [K \times (T)/Z]^{1/m}$, $a = n/m$, and n and m are Avrami and Ozawa exponents, respectively. The $F(T)$ has a physical meaning that a high value of $F(T)$ indicates low crystallization rate.[57] As shown in Figure 14 plotting log ϕ against log t for U[P(R)-HB]-40 and U[P(R)-HB]-40/3C composite demonstrates linear relationship at a given $X(t)$, and the values of log $F(T)$ and a are listed in Table V, in which $F(T)$ increases with the increase of the relative degree of crystallinity. There was a good linear relationship between log φ and log t.

Compared the values of log $F(T)$ of neat U[P(R)-HB]-40 with its composite at a given $X(T)$, it is obvious that the values of the U[P(R)-HB]-40/3C composite are higher than that of neat sample, suggesting a lower crystallization rate of the composite. The results are consistent with those of the crystallization half-time values and Z_c. The presence of chitin whiskers retards the crystallization of P[(R)-HB] in PUs.

The activation energy of crystallization for U[P(R)-HB]-40 and U[P(R)-HB]-40/3C composite can be evaluated with the Kissinger approach[62,63] as follows:

$$\ln\left(\frac{\phi}{T_p^2}\right) = \text{const.} - \frac{E_a}{RT_p}$$

where T_p is the maximum of melt crystallization peak at heating rate, ϕ. Therefore, the activation energy, E_a, can be determined from the slope of the plot of $\ln(\phi/T_p^2)$ versus $1/T_p$ (Figure 15). The calculated E_a values for the non-isothermal crystallization of pure U[P(R)-HB]-40 and its U[P(R)-HB]-40/3C composites are found to be 78.2 and 82.2 kJ/mol, respectively. These values suggest that the energy barrier is not significantly changed with the incorporation of chitin whisker in the polymer chains.

CONCLUSIONS

In summary, a series of biodegradable multiblock copolymers based on crystalline bacterial poly[(R)-3-hydroxybutyrate], P[(R)-HB], and amorphous chemo-synthetic poly[(R,S)-hydroxybutyrate] P[(R,S)-HB] with different compositions were successfully prepared and characterized. The incorporation of P[(R,S)-HB] segments retards the rate of crystallization of P[(R)-HB] segments in the copolymer. The thermal stability

of the copolymers increases with increasing the weight fraction of P[(R)-HB]. The copolymer containing ~40 wt % of P[(R)-HB], namely U[P(R)-HB]-40, loaded with various content of chitin wiskers (CW) ranging from 1 to 5% were prepared. The experimental results revealed that the incorporation of CW in the copolymer matrix slightly decreased the rate of crystallization of P[(R)-HB] segments and improved the thermal stability of the final copolymer composite. The non-isothermal melt crystallization of the neat U[P(R)-HB]-40 and its nanocomposite loaded with 3 % CW was studied. Avrami and Mo methods were successfully described the non-isothermal melt crystallization kinetics. The values of $t_{1/2}$ and Z_c indicated that the crystallization rate increases with increasing cooling rate for both copolymer and its composite. The presence of CW in the copolymer matrix restricts to some extent the motion of P[(R)-HB] segments; this results in slower crystallization.

In addition, the activation energy was calculated with Kissinger's method. The obtained value of composite was found to be higher than that of the neat sample.

The effect of the copolymer composition and the amount of CW incorporated within the copolymer on the non-isothermal crystallization is planned to be investigated in details in a future work.

In conclusion, our investigated copolymers seem to combine the criteria of biodegradability with improved thermal stability and wide processability window compared with high molecular weight P[(R)-HB]. In addition, such copolymers exihibit fast non isothermal melt crystallization to be excellent biodegradable polymers.

REFERENCES

1. Philip, S.; Keshavarz, T.; Roy, I. *J. Chem. Technol. Biot.* **2007**, *82*, 233.
2. Ojumu, T. V.; Yu, J.; Solomon, B. O. *Afr. J. Biotechnol.* **2004**, *3*, 18.
3. Pietrini, M.; Roes, L.; Patel, M. K.; Chiellini, E. *Biomacromolecules* **2007**, *8*, 2210.
4. Khanna, S.; Srivastava, A. K. *Process Biochem.* **2005**, *40*, 607.
5. Marchessault, R. H.; Okamura, K.; Su, C. J. *Macromolecules* **1970**, *3*, 735.
6. De Koning, G. J. M.; Lemstra, P. J. *Polymer* **1993**, *34*, 4089.
7. De Koning, G. J. M. *ACS Publ.* **1994**.
8. Doi, Y.; Kanesawa, Y.; Kunioka, M.; Saito, T. *Macromolecules* **1990**, *23*, 26.
9. Doi, Y.; Kitamura, S.; Abe, H. *Macromolecules* **1995**, *28*, 4822.
10. Asrar, J.; Valentin, H. E.; Berger, P. A.; Tran, M.; Padgette, S. R.; Garbow, J. R. *Biomacromolecules* **2002**, *3*, 1006.
11. Bordes, P.; Pollet, E.; Avérous, L. *Prog. Polym. Sci.* **2009**, *34*, 125.
12. El-Hadi, A.; Schnabel, R.; Straube, E.; Müller, G.; Henning, S. *Polym. Test* **2002**, *21*, 665.
13. Scandola, M.; Ceccorulli, G.; Pizzoli, M.; Gazzano, M. *Macromolecules* **1992**, *25*, 1405.
14. Yu, L.; Dean K.; Li, L. *Prog. Polym. Sci.* **2006**, *31*, 576.
15. Reeve, M. S.; McCarthy, S. P.; Downey, M. J.; Gross, R. A. *Macromolecules* **1994**, *27*, 825.
16. Hirt, T. D.; Neuenschwander, P.; Suter, U. W. *Macromol. Chem. Phys.* **1996**, *197*, 4253.
17. Lendlein, A.; Neuenschwander, P.; Suter, U. W. *Macromol. Chem. Phys.* **1998**, *199*, 2785.
18. Saad, G. R.; Lee, Y. J.; Seliger, H. *J. Appl. Polym. Sci.* **2002**, *83*, 703.
19. Liu, Q.; Cheng, S.; Li, Z.; Xu, K.; Chen, G. Q. *J. Biomed. Mater. Res. Part A* **2009**, *90*, 1162.
20. Saad, G. R.; Seliger, H. *Polym. Degrad. Stab.* **2004**, *83*, 101.
21. Naguib, H. F.; Aziz, M. S. A.; Sherif, S. M.; Saad, G. R. *J. Polym. Res.* **2011**, *18*, 1217.
22. Zhao, Q.; Cheng, G. *J. Mater. Sci.* **2004**, *39*, 3829.
23. Zhao, Q.; Cheng, G.; Li, H.; Ma, X.; Zhang, L. *Polymer* **2005**, *46*, 10561.
24. Zhao, Q.; Cheng, G.; Song, C.; Zeng, Y.; Tao, J.; Zhang, L. *Polym. Degrad. Stab.* **2006**, *91*, 1240.
25. Wang, S.; Song, C.; Chen, G.; Guo, T.; Liu, J.; Zhang, B.; Takeuchi, S. *Polym. Degrad. Stab.* **2005**, *87*, 69.
26. Lim, S. T.; Hyun, Y. H.; Lee, C. H.; Choi, H. J. *J. Mater. Sci. Lett.* **2003**, *22*, 299.
27. Bordes, P.; Pollet, E.; Bourbigot, S.; Averous, L. *Macromol. Chem. Phys.* **2008**, *209*, 1473.
28. Hablot, E.; Bordes, P.; Pollet, E.; Avérous, L. *Polym. Degrad. Stab.* **2008**, *93*, 413.
29. Bordes, P.; Hablot, E.; Pollet, E.; Avérous, L. *Polym. Degrad. Stab.* **2009**, *94*, 789.
30. D'Amico, D. A.; Manfredi, L. B.; Cyras, V. P. *Thermochim. Acta* **2012**, *544*, 47.
31. Yu, F.; Pan, P.; Nakamura, N.; Inoue, Y. *Macromol. Mater. Eng.* **2011**, *296*, 103.
32. Huang, X.; Li, C.; Guan, G.; Zhang, D.; Xiao, Y. *J. Appl. Polym. Sci.* **2010**, *118*, 2225.
33. Morin, A.; Dufresne, A. *Macromolecules* **2002**, *35*, 2190.
34. Zeng, J. B.; He, Y. S.; Li, S. L.; Wang, Y. Z. *Biomacromolecules* **2011**, *13*, 1.
35. Saad, G. R.; Lee, Y. J.; Seliger, H. *Macromol. Biosci.* **2001**, *1*, 91.
36. Gopalan Nair, K.; Dufresne, A. *Biomacromolecules* **2003**, *4*, 657.
37. Barham, P.; Keller, A. J.; Otun, E. L.; Holmes, P. A. *J. Mater. Sci.* **1984**, *19*, 2781.
38. Loh, X. J.; Wang, X.; Li, H. Z.; Li, X.; Li, J. *Mater. Sci. Eng. C* **2007**, *27*, 267.
39. Rodrigues, J. A.; Parra, D. F.; Lugao, A. B. *J. Therm. Anal. Cal.* **2005**, *79*, 379.
40. He, Y.; Shuai, X.; Cao, A.; Kasuya, K. I.; Doi, Y.; Inoue, Y. *Polym. Degrad. Stab.* **2001**, *73*, 193.
41. Pearce, R.; Marchessault, R. H. *Polymer* **1994**, *35*, 3990.
42. Barham, P. J.; Keller, A. *J. Polym. Sci. Pol. Phys.* **1986**, *24*, 69.

43. Kopinke, F. D.; Mackenzie, K. *J. Anal. Appl. Pyrol.* **1997**, *40*, 43.
44. Hariraksapitak, P.; Supaphol, P. *J. Polym. Sci.* **2010**, *117*, 3406.
45. Sriupayo, J.; Supaphol, P.; Blackwell, J.; Rujiravanit, R. *Carbohyd. Polym.* **2005**, *62*, 130.
46. Sriupayo, J.; Supaphol, P.; Blackwell, J.; Rujiravanit, R. *Polymer* **2005**, *46*, 5637.
47. Wu, X.; Torres, F. G.; Vilaseca, F.; Peijs, T. *J. Biobased Mater Bioenergy* **2007**, *1*, 341.
48. Yokouchi, M.; Chatani, Y.; Tadokoro, H.; Teranishi, K.; Tani, H. *Polymer* **1973**, *14*, 267.
49. Cobntbekt, J.; Mabchessault, R. H. *J. Mol. Biol.* **1972**, *71*, 735.
50. Minke, R. A. M.; Blackwell, J. *J. Mol. Biol.* **1978**, *120*, 167.
51. Cho, Y. W.; Jang, J.; Park, C. R.; Ko, S. W. *Biomacromolecules* **2000**, *1*, 609.
52. Jeziorny, A. *Polymer* **1978**, *19*, 1142.
53. Ozawa, T. *Polymer* **1971**, *12*, 150.
54. Xu, W.; Ge, M.; He, P. *J. Appl. Polym. Sci.* **2001**, *82*, 2281.
55. Wang, D. Y.; Wei, L. L.; Ge, X. G.; Yang, K. K.; Wang, X. L.; Wang, Y. Z. *J. Macromol. Sci. Part B: Phys.* **2009**. *48*, 927.
56. Zheng, G. C.; Ding, S. D.; Zeng, J. B.; Wang, Y. Z.; Li, Y. D. *J. Macromol. Sci. Part B: Phys.* **2010**, *49*, 269.
57. Liu, T., Mo, Z.; Wang, S.; Zhang, H. *Polym. Eng. Sci.* **1997**, *37*, 568.
58. Zeng, J. B.; Liu, C.; Liu, F. Y.; Li, Y. D.; Wang, Y. Z. *Ind. Eng. Chem. Res.* **2010**, *49*, 9870.
59. Lu, J. S.; Chen, M.; Lu, S. F.; Chen, C. H. *J. Polym. Res.* **2011**, *18*, 1527.
60. Tang, C. Y.; Chen, D. Z.; Tsui, C. P.; Uskokovic, P. S.; Yu, P. H.; Leung, M. C. *J. Appl. Polym. Sci.* **2006**, *102*, 5388.
61. Duan, B.; Wang, M.; Zhou, W. Y.; Cheung, W. L. *Polym. Eng. Sci.* **2011**, *51*, 1580.
62. Bhattarai, N.; Kim, H. Y.; Cha, D. I.; Lee, D. R.; Yoo, D. I. *Eur. Polym. J.* **2003**, *39*, 1365.
63. Choi, J.; Chun, S. W.; Kwak, S. Y. *Macromol. Chem. Phys.* **2006**, *207*, 1166.